Static dielectric permittivity of ionic liquids ultraconfined in carbon nanotubes

Nadia Ben Chiekh Mansour, M.-L. Ouinten, Armand Soldera, Anthony Szymczyk, Aziz Ghoufi

Static dielectric permittivity of ionic liquids ultraconfined in carbon nanotubes

NANO EXPRESS

PAPER

Static dielectric permittivity of ionic liquids ultraconfined in carbon nanotubes

Nadia Ben Cheick Mansour[1], **Mohammed-Lamine Ouiten**[1,2], **Armand Soldera**[3], **Anthony Szymczyk**[2] and **Aziz Ghoufi**[1]

[1] Institut de Physique de Rennes, IPR, CNRS-Université de Rennes 1, UMR CNRS 6251, 35042 Rennes, France
[2] Univ Rennes, CNRS, ISCR (Institut des Sciences Chimiques de Rennes), UMR 6226, F-35000 Rennes, France
[3] Laboratory of Physical Chemistry of Matter (LPCM), Department of Chemistry, Université de Sherbrooke, Sherbrooke, J1K 2R- Québec, Canada

E-mail: aziz.ghoufi@univ-rennes1.fr

Keywords: Ionic liquids, confinement, dielectric properties, molecular dynamics simulations

OPEN ACCESS

RECEIVED
31 December 2020

REVISED
26 February 2021

ACCEPTED FOR PUBLICATION
9 March 2021

PUBLISHED
18 March 2021

Abstract

In this work the parallel component of the static dielectric permittivity, ϵ_{II} of ionic liquids ultraconfined into flexible carbon nanotubes of radius of 1.2 nm and 2.4 nm is evaluated from molecular dynamics simulations. We show an enhancement of ϵ_{II} with respect to bulk value and a counter-intuitive temperature dependence. Indeed an increase of ϵ_{II} as a function of the temperature opposed to a bulk behavior is evidenced. Increase in ϵ_{II} is the result of the strong orientation of ionic liquid close to the pore wall. The temperature dependence is the consequence of the thermal fluctuations increasing the dipolar fluctuations such that the strong orientation is conserved. Eventually, we show a molecular stacking between $[C_4mim^+][Tf_2N^-]$ and CNT decreasing dipolar fluctuations close to the CNT surface reducing ϵ_{II}.

1. Introduction

Ionic Liquids (ILs) are molten salts composed of large organic cations and inorganic or organic anions. ILs are widely studied given their applications [1, 2] associated with their physical properties such as negligible vapor pressure, thermal stability, high ionic conductivity, etc. Over the last few years, the confinement of ILs at the nanoscale has gained much attention given their applications as electrochemical double-layer capacitors (EDLCs) [1–5]. ILs are also considered as potential lubricants [6] when confined into nanoporous materials such as carbon nanotubes (CNTs) [7]. The macroscopic performance of nanoconfined ILs is thus controlled by their physical properties at the nanoscale [8–10], that are deviated from the bulk phase. Determination and understanding of the physical properties at the molecular scale of confined ILs is then critical for the rational design of industrial processes with optimal properties.

Several works on the ILs confined into cylindrical nanopores, such as CNTs [9, 11–18], silica materials [19–21], rutile slabs [22] and graphitic pores [8], suggested that both local ILs structure and dynamics of confined cations and anions are very complex and heterogeneous, depending strongly on the distance between ions and the pore wall. Furthermore, CNTs represent a perfect model of nanopores allowing to explore confinement effects on the structural organization and the dynamical properties of complex and molecular liquids. Some interesting properties were thus reported for various liquids confined into CNTs such as fast transport [16, 23–27], small friction [23, 25], increase in dielectric permittivity [28], etc.

While structure, dynamics and electrical properties of confined ILs were strongly examined their dielectric properties have been poorly studied. Among them, the static dielectric constant (ϵ) that characterizes the capacity of a material to transmit an electric field and controls the charge migration and dipole reorientation is probably one of the more important properties in context of capacitors and fuel cell batteries. Electrical double layer capacitors are part of super-capacitors storing charges on the surface of electrode materials. When a cell voltage is applied, the ions electrostatically adsorbed at the electrode/electrolyte interface contribute to the

charge stored by EDLCs. Theoretically, the Poisson-Boltzmann (PB) equation allows us to describe the electric potential (Ψ) of a charge distribution. In this context, Ψ is connected to the relative dielectric permittivity (or static dielectric constant) from $\frac{d^2\Psi}{dz^2} = -\frac{\rho}{\epsilon_0 \epsilon}$ where ρ is the volume charge density and ϵ_0 is the vacuum permittivity. Resolution of PB equation allows to define the Debye length ($\lambda_D = \sqrt{\frac{\epsilon_0 \epsilon k_B T}{2e^2 n_\infty}}$, where T is the temperature, k_B is the Boltzmann's constant, e is the elementary charge and n_∞ is the concentration in volume) that is a measure of a charge carrier's net electrostatic effect in a solution and how far its electrostatic effect persists. As shown by the above equation, λ_D obviously depends on the relative dielectric permittivity of the medium.

Up to now, theoretical and numerical studies assumed that the dielectric permittivity of confined IL was similar to the bulk value but several recent works showed the opposite [28–32]. Indeed, an increase of the dielectric permittivity of confined water into carbon nanotubes was highlighted [28–32] while anomalous dielectric constant of confined electrolytic solutions was evidenced [33, 34]. Recently, a few studies were undertaken to gain insight into the dielectric properties of water inside different confining media such as carbon nanotubes (CNTs)[35–37], graphene nanosheets [30, 38] and porous silica membranes. [29, 31, 33, 39, 40]. For instance, Netz *et al* showed a local interfacial increase in the axial (tangential) component of the dielectric constant ($\epsilon_{||}$) close to both hydrophobic and hydrophilic planar interfaces [38, 41]. This enhancement of interfacial $\epsilon_{||}$ was confirmed by Galli *et al* who focused on the dielectric behavior of water confined between two graphene nanosheets [30]. These works were completed by several studies on the dielectric properties of water confined into cylindrical hydrophilic silica nanopores [29, 31, 33, 39, 40] and hydrophobic CNTs [31]. In a cylindrical nanopore, a dielectric anisotropy was observed between the radial and axial components of the dielectric tensor with a much larger value of $\epsilon_{||}$. These predictions were validated by some experiments performed with water confined into a 1D-channel molecular crystal and CNT that led to similar qualitative conclusions [42, 43].

These works have evidenced that the dielectric permittivity of confined liquids differs from the bulk counterpart and is strongly dependent on the position with respect to the pore wall. The impact of confinement on the dielectric properties of ILs has never been explored so far and the lack of knowledge about the dielectric constant of confined ILs strongly limits our ability to model fluid-material interactions and more generally our understanding of the dielectric behavior of confined ILs. This fundamental issue is addressed in the present work by means of Molecular Dynamics (MD) simulations of $[BuMe_3N^+][Tf_2N^-]$ and $[C_4mim^+][Tf_2N^-]$ ILs confined in CNTs of radius 1.2 nm (CNT(20,20)) and 2.4 nm (CNT(40,40)).

2. Methods

Computational procedure and force field

As shown in figure 1, $BuMe_3N^+$ and Tf_2N^- ions were described by using the united atom OPLS force field [44]. $[C_4mim^+][Tf_2N^-]$ IL was modeled from a recent united atom force field [45]. The CNT material was modeled as non-charged and flexible from the Tersoff potential [46]. A perfect (without defaults) flexible armchair-typed CNT with a radius of 1.2 nm and a length of 100 Å was considered corresponding to 3280 carbon atoms. A length of 10 nm was considered to avoid the size effect [47] that corresponds to 100 carbon atoms per nm length of CNT [48].

All MD simulations were carried out with the DL_POLY package (version 4.0) [49] using a combination of the velocity-Verlet and the SHAKE-RATTLE algorithms [50]. The Nose-Hoover thermostat [51, 52] with a relaxation time of $\tau_t = 0.5$ ps was considered. Periodic boundary conditions were applied in the three directions. MD simulations were performed in the canonical ensemble (NVT, where N is the number of ions, V is the volume and T is the temperature) at T = 330 K and T = 450 K. MD simulations were performed using a time step of 0.001 ps to sample 100 ns (acquisition phase) after a 100 ns equilibration. Electrostatic interactions were truncated at 12 Å and calculated by using the Ewald sum with a precision of 10^{-6}. Short range interactions were modeled by using a Lennard-Jones potential and a cutoff of 12 Å. Lennard-Jones interactions between CNT and ionic liquids have been taken into account by means of the Lorentz-Berthelot mixing rule. Statistical errors were estimated using the block average method. Comparisons between bulk and confined properties were performed at $p = 1$ bar. MD simulation of bulk liquid phase was carried out in NpT ensemble from the Nose-Hoover barostat using a relaxation time of 0.1 ps.

Density of confined ILs was computed by means of an anisotropic barostat [53] by contacting the empty CNT with two RTIL reservoirs at 1bar. Simulation box dimensions were Lx = Ly = 100 Å and Lz = 300 Å. This method was used to calculate the density of confined IL at 330 K and 450 K. 77 and 76 ions pairs were found at 330 K and 450 K, respectively highlighting a small impact of the temperature on the confined IL density. After convergence of the confined IL density, MD simulations of a CNT without external reservoirs were carried out

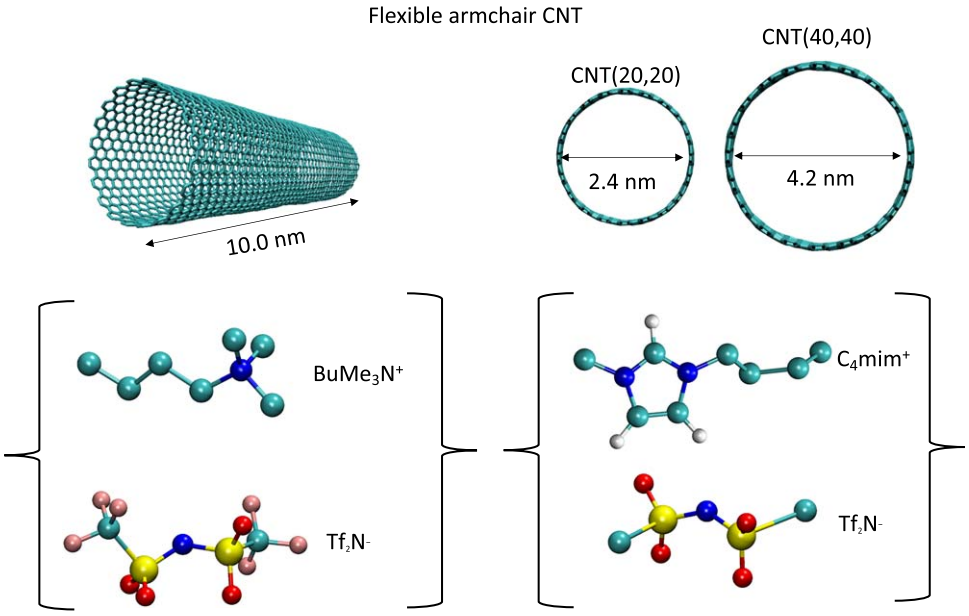

Figure 1. Illustration of flexible carbon nanotube and the united atom description of $[BuMe_3N^+][Tf_2N^-]$ and $[C_4mim^+][Tf_2N^-]$ ILs. Carbon, oxygen, hydrogen, sulfur and fluorine atoms are represented in cyan, red, white, yellow and pink colors, respectivley.

with simulation box dimensions Lx = Ly = 30 Å and Lz = 100 Å .This configuration was equilibrated in the canonical ensemble for 100 ns.

Dielectric permittivity calculation

In a cylindrical nanopore the dielectric permittivity is described as a tensor varying with the position with respect to the pore wall involving thus a radial dependance ϵ (r) given the radial symmetry. Calculation of the profile of the local static dielectric permittivity was already investigated under cylindrical [33, 39], spherical [29, 54] and planar [29, 38, 54] confinements. As emphasized in [29, 38, 39, 54] such a task requires to know the symmetry of the system. In a cylindrical nanopore the liquid is confined in the radial direction while no confinement effect is expected in the *z* direction. From the linear dielectric response and the fluctuation theorem it has been established in [33, 39] that the parallel dielectric permittivity could be evaluated as $\epsilon_{||}(r) = 1 + \beta\epsilon_0^{-1}[\langle m_{||}(r)M_{||}\rangle_0 - \langle m_{||}(r)\rangle_0\langle M_{||}\rangle_0]$ where $< ... >_0$ denotes a statistical ensemble average in absence of the external field, || corresponds to axial direction along to the *z* directions, β is the reverse temperature, ϵ_0 is the dielectric vacuum permittivity , $m_{||}(r)$ is the local dipolar moment in the axial direction, $M_{||}$ is the total dipolar moment in the axial direction defined as $\mathbf{M}_{||} = \int_V \mathbf{m}_{||}(\mathbf{r})d\mathbf{r}$. Let us note that moments of order higher than two were not taken into account because it was shown that they have a negligible impact on the value of ϵ (*r*) in cylindrical nanopores [39]. In this work the orthogonal component was not evaluated because it was shown that its value was much smaller than that of the parallel component [55, 56].

3. Results and discussions

We report in figure 2(a) the profile of $\epsilon_{||}(r)$ for $[BuMe_3N^+][Tf_2N^-]$ confined in the CNT(20,20) for two different temperatures T. Let us note that the nanotube was divided in cylindrical shells of position r varying from 0 to the pore radius (1.2 nm) such that $r = \sqrt{(}x^2 + y^2)$ where x and y are the positions of the centre of mass of the ions. Figure 2(a) evidences the fact that the dielectric permittivity of confined IL is a function of the radial position into the nanotube. Furthermore figure 2(a) highlights an increase in the dielectric permittivity with respect to the bulk phase (6.11 ± 0.02 at 450 K). At room temperature i.e. at 300 K the experimental value is 12.5 [57]. Interestingly a large part of ILs and virtually all molecular liquids show a negative value of $d\epsilon/dT$ [58]. Indeed, the decrease in the number density of their dipoles with increasing T predominates over the temperature-induced decrease in antiparallel dipole−dipole correlations. From [58] $d\epsilon/dT$ is around 0.05 K^{-1} that allowed us to estimated a loss of 7.6 in ϵ at 450 K with respect to 300 K i.e. a dielectric constant of 4.9, which is in fair agreement with the calculated value (6.11). To ensure the absence of dipolar correlation at *r* and then to validate the calculation of $\epsilon_{||}(r)$ the correlation function $C(r, t) = <m_{||}(r, t)M_{||}(t).m_{||}(r, 0)M_{||}(0) > / < m_{||}(r, 0)M_{||}(0)>$ was calculated. We report in figure 2(b) C(r, t) calculated at r = 9.8 Å corresponding to the maximum of $\epsilon_{||}(r)$ for both temperatures (330 K and 450K).

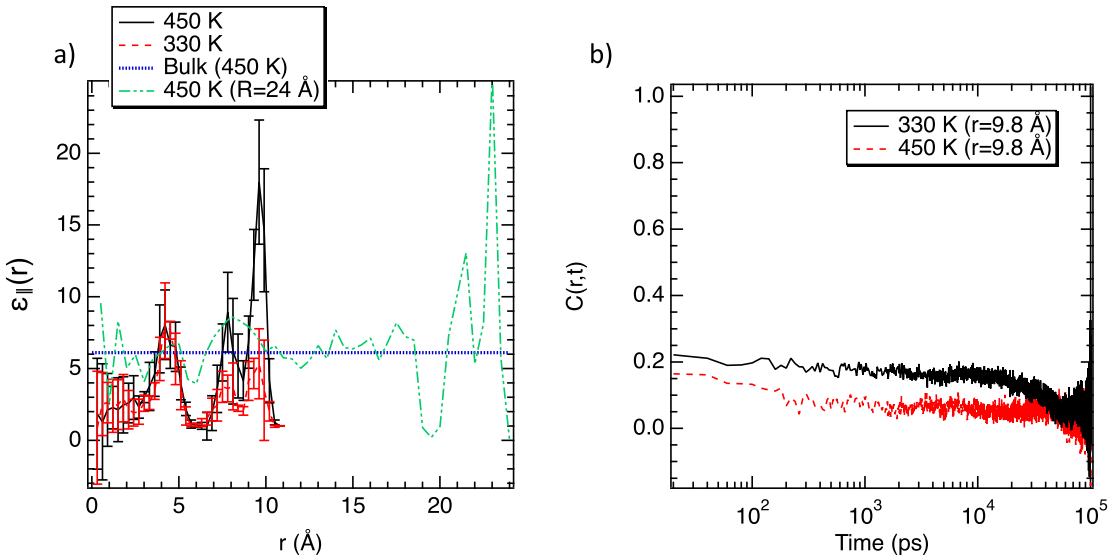

Figure 2. (a) Axial static dielectric permittivity ($\epsilon_{||}(r)$) of [$BuMe_3N^+$][Tf_2N^-] confined in the CNT(20,20) as a function of *r* and T. The horizontal dotted line represents the dielectric permittivity in bulk phase. (b) Correlation function C(r,t) of [$BuMe_3N^+$][Tf_2N^-] at 330 K and 450 K at r = 9.8 Å corresponding to the maximum of $\epsilon_{||}(r)$.

Figure 2(b) shows a fast decay of C(r,t) highlighting decorrelated dipolar moment in the axial direction, which validates the calculation of $\epsilon_{||}(r)$.

The physical properties of confined fluids are often correlated to their local density. We report in figure 3 the density profile of the centre of mass of ions as a function of *r* for both 330 K and 450 K temperatures. Figures 3(a) and 3(b) suggests that the local dielectric permittivity is correlated to the local density. Indeed, this figure shows that the maxima in the dielectric permittivity and density are located at the same positions. The increase in $\epsilon_{||}(r)$ could be then connected to the increase in density. We have then modeled a bulk system with a density corresponding to the 0.016 molecule/Å^3 i.e. the maximum of density observed in figure 3a. After 100 ns of equilibration in NVT statistical ensemble the dielectric permittivity was found close to 5.9 that suggests that the increase in density is not at the origin of the high $\epsilon_{||}(r)$. We report in figures 3(c) and 3d the dielectric contribution of both $BuMe_3N^+$ and Tf_2N^- ions. These figures show that both maxima of $\epsilon_{||}(r)$ at r = 4 Å and close to the CNT surface (r = 9.8 Å) can be attributed to the cation $BuMe_3N^+$ while the peak observed at r = 8 Å is related to Tf_2N^-. Furthermore figures 3(c) and 3d show that the ions are organized in successive shells from the CNT surface; $BuMe_3N^+$-Tf_2N^--$BuMe_3N^+$ forming an electrical double layer although the CNT is uncharged. This organization is the consequence of both excluded volume [59, 60] and the hydrophobic interactions between CNT material and carbon atoms of $BuMe_3N^+$ [27].

The static dielectric permittivity is a measure of the ability of molecules to orientate themselves along the direction imposed by an external electrical field. In a confined environment the dielectric permittivity could be connected to the orientation of molecules in the absence of an electrical field [27]. We report in figure 4 the distribution of the angle (Φ) between the dipolar moment vector of $BuMe_3N^+$ and Tf_2N^- and the unit vector according to the *z* direction close to the solid surface. Figure 4 shows that the $BuMe_3N^+$ cation is strongly oriented in the CNT whatever the temperature. Indeed, figure 4 highlights preferential angles of 10^o and 170^o suggesting dipolar moment vector of $BuMe_3N^+$ is oriented in the axial direction. This strong pre-orientation is at the origin of increase of dielectric permittivity because it facilitates the orientation of ions when an electrical field is applied. Figure 4 depicts that, although all angles are well sampled, Tf_2N^- is also preferentially oriented according to the *z* direction, 45, 90 and 135^o but to lesser extent than $BuMe_3N^+$. These results are in good agreement with figure 3(b) showing that the dielectric permittivity contribution of Tf_2N^- is weaker than $BuMe_3N^+$. Moreover, figure 4 highlights that this strong orientation is kept despite the increase in temperature. The thermal energy is not enough to surpass the induced order due to the ultraconfinement at the nanoscale.

The temperature dependence of $\epsilon_{||}(r)$ could be imputed to an increase in dipolar fluctuations as the temperature increase. Indeed, the additional thermal energy at 450 K leads to a slight increase of thermal fluctuation without altering the strong orientation observed in figure 4. As shown in figure 5 that leads to an increase in dipolar fluctuations ($\delta\epsilon_{||}(r)$). Indeed, figure 5 highlights that the dipolar fluctuations are higher at 450 K that is line with the figure 2. These results shed light on the existence of an interplay between strong order caused by the extreme confinement and disorder triggered by the thermal fluctuations. In bulk phase the

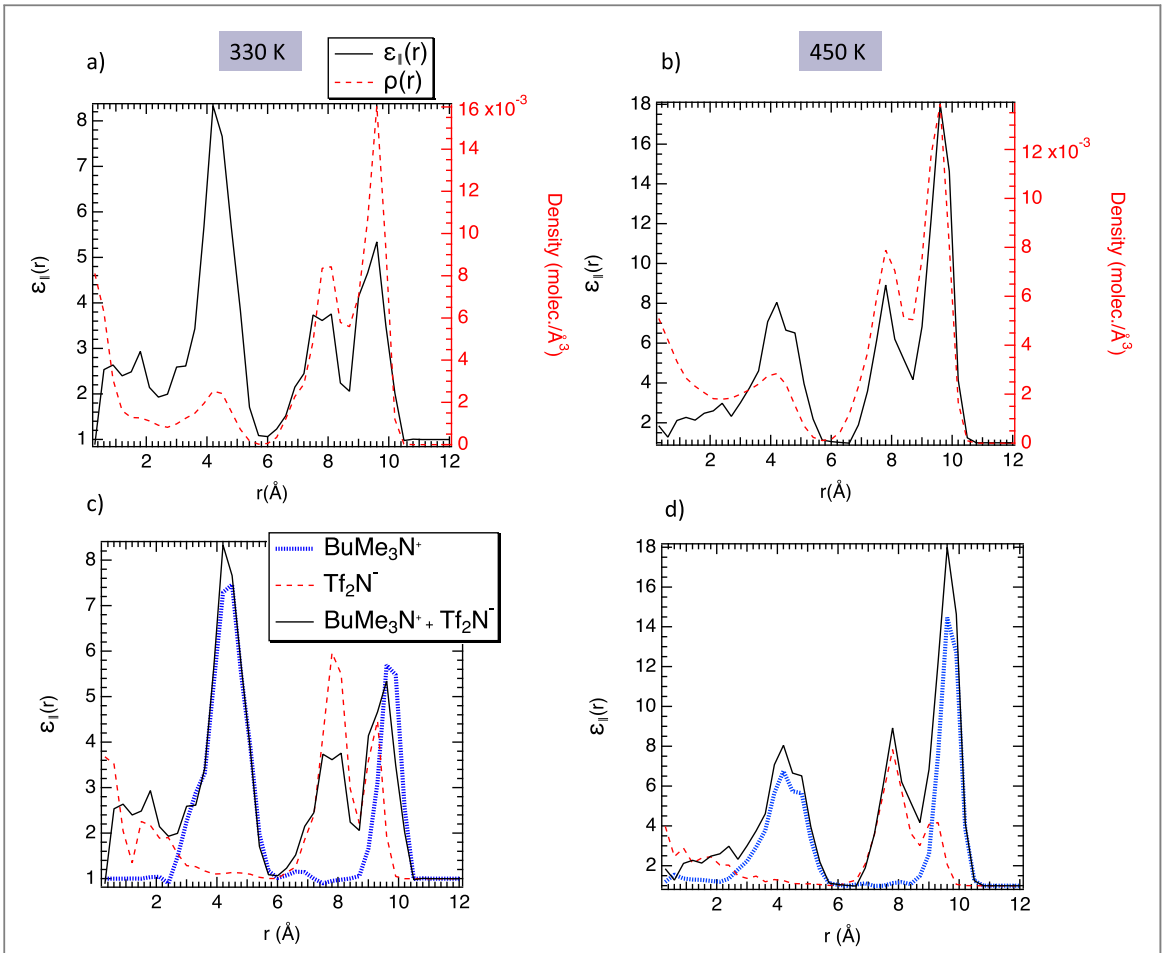

Figure 3. Axial static dielectric permittivity ($\epsilon_{||}(r)$) and profile of density ($\rho(r)$) of [$BuMe_3N^+$][Tf_2N^-] as a function of r at 330 K (a) and 450 K (b). Dielectric contribution of both $BuMe_3N^+$ and Tf_2N^- ions at 330 K (c) and 450 K (d).

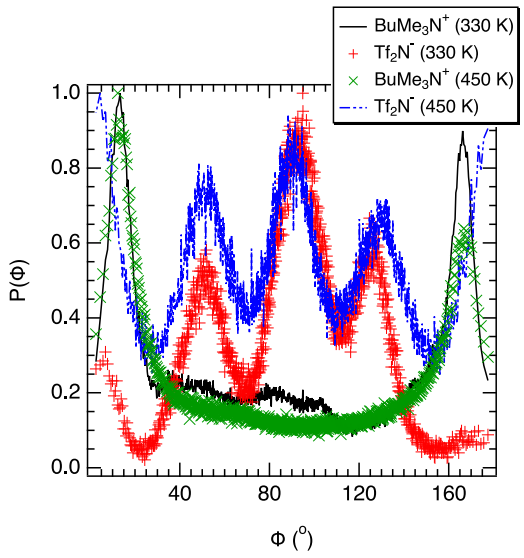

Figure 4. Distribution of the angle (Φ) between the dipolar moment vector of $BuMe_3N^+$ and Tf_2N^- and the unit vector according to the z direction for two temperatures 330 K and 450 K.

increase in temperature leads to a disorder decreasing the orientation processus under electrical field involving then a decrease in dielectric permittivity.

The confinement effect on ILs was also examined from MD simulations of confined [C_4mim^+][Tf_2N^-] at 400 K. Confined density of [C_4mim^+][Tf_2N^-] was calculated from the method detailed in section 2. Contrary to

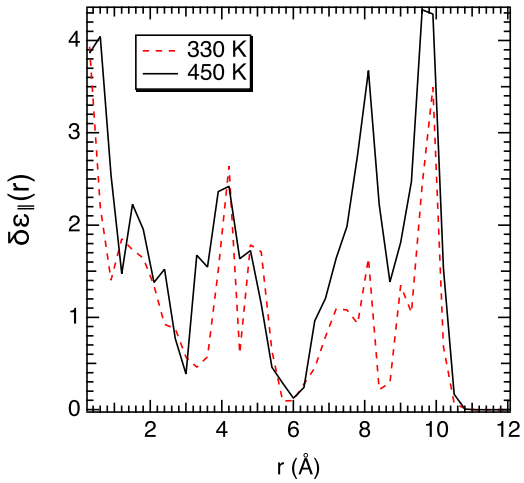

Figure 5. Dipolar fluctuations ($\delta\epsilon_{||}(r)$) of confined [$BuMe_3N^+$][Tf_2N^-] as a function of the radial position (r) at 330 K and 450 K.

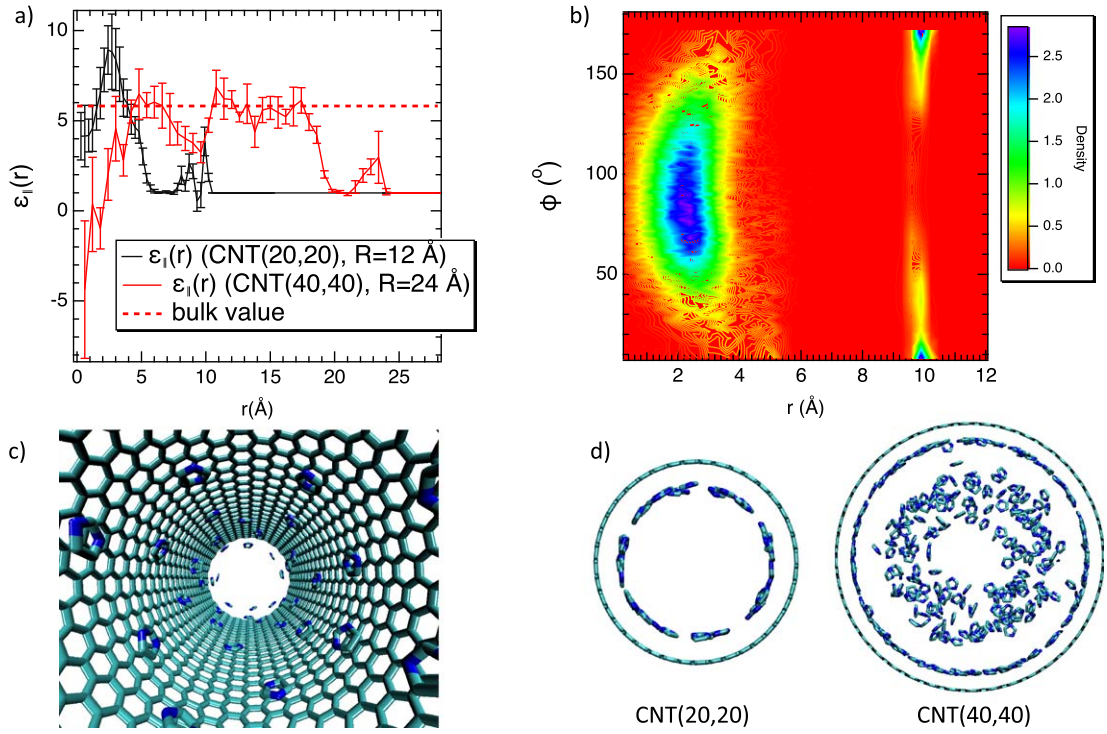

Figure 6. (a) $\epsilon_{||}(r)$ of [C_4mim^+][Tf_2N^-] confined in CNT(20,20) and CNT(40,40) at 400 K. (b) Two dimensional density of the angle between the dipolar vector of C_4 mim^+ as a function of the radial distance. (c) Snapshot of the confined C_4mim^+ close to the surface. For clarity, only the imidazole cycle is represented. (d) Snapshot of C_4mim^+ confined in CNT(20,20) and CNT(40,40).

$BuMe_3N^+$, C_4mim^+ has an imidazole ring that enables molecular stacking with the aromatic cycles of CNT [27]. As shown In figure 6(a) an increase in $\epsilon_{||}(r)$ with respect to the bulk phase is also observed that confirms the confinement effect on the static dielectric permittivity of IL. Contrary to the [$BuMe_3N^+$] [Tf_2N^-], the maximum of $\epsilon_{||}(r)$ is observed at the centre of pore suggesting that a decrease in dipolar fluctuations of ions close to the solid surface. The orientation of C_4mim^+ as a function of the radial position is reported in figure 6b. This figure shows a preferential orientation close to the solid surface and at the centre of pore. Despite the strong interfacial orientation the dielectric permittivity is lower than to the bulk value. That could be explained by a strong anchoring of C_4mim^+ at the CNT surface that counteracts the dipolar fluctuations. Indeed, figure 6(c) highlights a molecular stacking between the imidazole rings of C_4mim^+ and the aromatic cycle of CNT. This commensurate organization decreases the dipolar degree of freedom at the origin of the decrease in $\epsilon_{||}(r)$. Eventually, pore size effect was investigated from the confinement of [C_4mim^+][Tf_2N^-] at 400K into the CNT (40,40) material with a pore radius of 24 Å. As shown in figure 6(a) $\epsilon_{||}(r)$ of IL confined in CNT(40,40) is close to

the bulk value. For a pore radius of 24 Å the confinement does not affect the dielectric permittivity although the cation C_4mim^+ is still well anchored close to the CNT(40,40) surface as near to the CNT(20,20) interface (Figure 6d). Given the interfacial molecular staking between cations and the CNT, $\epsilon_{||}(r)$ is then similar in both CNT(40,40) and CNT(20,20). At the centre of the CNT(40,40) IL recovers a bulk like behavior due to weak confinement effect. Recently it has been shown that the bulk trend at the centre of pore and the interfacial enhancement of the physical properties were recovered from a pore radius of 20 Å [28] that is in line with the result observed in figure 6. A recent work suggests that the confinement and the interfacial effects are lost from a pore radius of 2000nm [61]. As shown in figure 2(a) this behavior is also observed from confined $[BuMe_3N^+][Tf_2N^-]$ within CNT(40,40). The interfacial structure is then independent on the stacking organization but is rather the consequence of the excluded volume.

4. Conclusion

In this work the parallel static dielectric permittivity ($\epsilon_{||}(r)$) of confined ionic liquids into the carbon nanotubes was investigated from molecular dynamics simulations. By calculating $\epsilon_{||}(r)$ from the fluctuation theorem we have established an enhancement with respect to the bulk value. We evidenced that this increase in $\epsilon_{||}(r)$ was the result of the strong orientation of ions into CNT allowing easier alignement along the unconfined axis under electrical field. This orientation is the result of the ultra-confinement propagating the interfacial orientation to the centre of pore. This increase in $\epsilon_{||}(r)$ was verified for both $[BuMe_3N^+][Tf_2N^-]$ and $[C_4mim^+][Tf_2N^-]$ ILs confined into CNT(20,20) material. The temperature dependence on $\epsilon_{||}(r)$ was also examined. Counterintuitively, we have highlighted that an increase in temperature led to an increase in $\epsilon_{||}(r)$. Indeed, the thermal fluctuations increase the dipolar orientation without breaking the strong orientation of confined ions. With $[C_4mim^+][Tf_2N^-]$ we exhibited a molecular staking where the imidazole cycles were commensurate with the aromatic cycles of CNT. This strong interactions led to a strong anchoring and then a decrease in dipolar fluctuations and a reduction in the interfacial $\epsilon_{||}(r)$ with respect to $[BuMe_3N^+][Tf_2N^-]$. Eventually, pore size effect was also investigated by studying the confinement of $[C_4mim^+][Tf_2N^-]$ into the CNT(20,20) and CNT (40,40) of pore radius of 12 Å and 24 Å. We showed that the increase in $\epsilon_{||}(r)$ wore off as the pore size increased because the volume effects surpassed the surface ones and the bulk trend was recovered.

Acknowledgments

The authors are grateful to the 'CNRS' for its financial support through the programs PEPS Infinity and PICS Waterloo. The 'Agence Nationale de la Recherche' is also acknowledged for its financial support through the program MANIAC.

ORCID iDs

Aziz Ghoufi https://orcid.org/0000-0003-0877-7968

References

[1] Plechkova N and Seddon K 2008 *Chem. Soc. Rev.* **37** 123
[2] Armand M, Endres F, MacFarlane D, Ohno H and Scrosati B 2009 *Nat. Mater.* **8** 621
[3] Zhang L and Zhao X 2009 *Chem. Soc. Rev.* **38** 2520
[4] Simon P and Gogotsi Y 2008 *Nat. Mater.* **7** 845
[5] Arico A, Bruce P, Scrosati B, Tarascon J and Schalkwijik W V 2005 *Nat. Mater.* **4** 366
[6] Zhou F, Liang Y and Liu W 2009 *Chem. Soc. Rev.* **38** 2590
[7] Ducros J, Buchtova N, Magrez A, Chauvet O and bideau J L 2011 *J. Mater. Chem.* **21** 2508
[8] Rajput N N, Monk J, Sing R and Hung F 2012 *J. Phys. Chem.* C **116** 5169
[9] Feng G, Li S, presser V and Cummings P 2013 *J. Phys. Chem. Letters* **4** 3367
[10] Alba-Simionesco C, Coasne B, Dosseh G, Dudziak G, Gubbins K, Radhakrishnan R and Sliwinska-Bartkowiak M 2006 *J. Phys. Condens. Matter* **18** R15
[11] Fukushima T and Aida T 2007 *Chemistry* **13** 5048
[12] Yang L, Fishbine B, Migliori A and Pratt L 2009 *J. Am. Chem. Soc.* **131** 12373
[13] Shim Y and Kim H 2009 *ACS Nano* **3** 1693
[14] Shim Y and Kim H 2010 *ACS Nano* **4** 2345
[15] Frolov A, Kirchner K, Kirchner T and Fedorov M 2012 *Faraday Discuss.* **154** 235
[16] Chaban V and Prezhdo O 2014 *ACS Nano* **8** 8190
[17] Shin J H, Kim G H, Kim I, Jeon H, An T and Lim G 2015 *Sci. Rep.* **5** 11799
[18] Orhan M, Kinaci A and Cagin T 2020 *Chem. Phys.* **530** 110598
[19] Li S, Han K, Feng G, Hagaman E, Vlcek L and Cummings P 2013 *Langmuir* **29** 9744
[20] Gupta A K, Verma Y L, Singh R K and Chandra S 2014 *J. Phys. Chem.* C **118** 1530

[21] Ori G, Villemot F, Viau L, Vioux A and Coasne B 2014 *Mol. Phys.* **112** 1350
[22] Liu L, Li S, Cao Z, Peng Y, Li G, Yan T and Gao X 2007 *J. Phys. Chem.* C **111** 12161
[23] Falk K, Sedlmeier F, Joly L, Netz R and Bocquet L 2010 *Nano. Lett.* **10** 4067
[24] jobic H, Rosenbach N, Ghoufi A, Kolokolov D, Yot P, Devic T, Serre C, Férey G and Maurin G 2010 *Chemistry-A Eur. J.* **16** 10337
[25] Falk K, Sedlmeier F, Joly L, Netz R and Bocquet L 2012 *Langmuir* **28** 14261
[26] Rosenbach N, Jobic H, Devic T, Koza M, Ramsahye N, Mota C, Serre C and Maurin G 2014 *J. Phys. Chem. C* **118** 14471
[27] Ghoufi A, Szymczyk A and Malfreyt P 2016 *Sci. Rep.* **6** 28518
[28] Renou R, Szymczyk A, Maurin G, Malfreyt P and Ghoufi A 2015 *J. Chem. Phys.* **142** 4
[29] Ghoufi A, Szymczyk A, Renou R and Ding M 2012 *EPL* **99** 37008
[30] Zhang C, Gygi F and Galli G 2013 *J. Phys. Chem. Letters* **4** 2477
[31] Renou R, Szymczyk A, Maurin G and Ghoufi A 2014 *Mol. Sim.* **41** 483
[32] Motevaselian M and Aluru N 2020 *J. Phys. Chem. Letters* **11** 10532–7
[33] Zhu H, Ghoufi A, Szymczyk A, Balannec B and Morineau D 2013 *Phys. Rev. letters* **109** 107801
[34] Renou R, Szymczyk A and Ghoufi A 2015 *Nanoscale* **7** 6661
[35] Lin Y, Shiomi J, Maruyama S and Amberg G 2009 *Phys. Rev.* B **80** 045419
[36] Mikami F, Matsuda K, Kataura H and Maniwa Y 2009 *ACS Nano* **3** 1279–87
[37] Qi W, Chen J, Lei X, Song B and Fang H 2013 *J. Phys. Chem.* B **117** 7967
[38] Bonthuis D J, Gekle S and Netz R R 2011 *Phys. Rev. Lett.* **107** 166102
[39] Zhu H, Ghoufi A, Szymczyk A, Balannec B and Morineau D 2013 *Phys. Rev. Letters* **111** 089802
[40] Renou R, Ghoufi A, Szymczyk A, Zhu H, Neyt J C and Malfreyt P 2013 *J. Phys. Chem.* C **117** 11017
[41] Bonthuis D, Gekle S and Netz R 2012 *Langmuir* **28** 7679
[42] Cui H B, Takahashi K, Okano Y, Kobayashi H, Wang Z and Kobayashi A 2005 *Angew. Chem.* **117** 6666
[43] Chen Qi. J., Yang J, Lei J, Lei X, Song Bo and Fang H 2014 *J. Phys. Chem.* B **117** 7967
[44] Jorgensen W, Maxwell D and Tirado-Rives J 1996 *J. Am. Chem. Soc.* **118** 11225
[45] Zhong X, Liu Z and Cao D 2011 *J. Phys. Chem.* B **115** 10027
[46] Tersoff J 1988 *Phys. Rev.* B **37** 6991
[47] Renou R, Szymczyk A and Ghoufi A 2014 *Mol. Phys.* **112** 2275
[48] Yuan Q, Xu Z, Yakobson B L and Ding F 2012 *Phys. Rev. Lett.* **108** 245505
[49] Todorov I, Smith W, Trachenko K and Dove M 2006 *J. Mater. Chem.* **16** 1911
[50] Allen M P and Tildesley D J 1987 *Computer Simulations of Liquids* (New York, NY: Oxford)
[51] Nose S 1984 *J. Chem. Phys.* **81** 511
[52] Hoover W 1985 *Phys. Rev.* A **31** 1695
[53] Ghoufi A, Morineau D, Lefort R, Hureau I, Hennous L, Zhu H, Szymczyk A, Malfreyt P and Maurin G 2011 *J. Chem. Phys.* **134** 074104
[54] Ballenegger V and Hansen J P 2005 *J. Chem. Phys.* **122** 114711
[55] Mondal S and Bagchi B 2019 *J. Phys. Chem. Letters* **10** 6287
[56] Motevaselian M and Aluru N 2020 *ACS Nano* **14** 12761
[57] Weingärtner H, Sasisanker P, Daguenet C, Dyson P, Krossing I, Slattery J M and Schubert T 2007 *J. Phys. Chem.* B **111** 4775
[58] Hunger J, Stoppa A, Schrodle S, Hefter G and Buchner R 2009 *Chem. Phys. Chem.* **10** 723
[59] Morineau D, Guégan R, Xia Y and Alba-Simionesco C 2004 *J. Chem. Phys.* **121** 1466
[60] Ghoufi A, Hureau I, Morineau D, Renou R and Szymczyk A 2013 *J. Phys. Chem.* C **117** 15203
[61] Morikawa K, Kazoe Y, Mawatari K, Tsukahara T and Kitamori T 2015 *Anal. Chem.* **87** 1475